ELSEVIER

Journal of Applied Geophysics 42 (1999) 283–300

JOURNAL OF APPLIED GEOPHYSICS

www.elsevier.nl/locate/jappgeo

Application of multifocusing method for subsurface imaging

Evgeny Landa *, Boris Gurevich [1], Shemer Keydar, Pinchas Trachtman

The Geophysical Institute of Israel, PO Box 182, Lod 71100, Israel

Abstract

The multifocusing method consists of stacking seismic data with arbitrary source–receiver distribution according to a new paraxial moveout correction. This multifocusing moveout correction is based on a local spherical approximation of the reflection wave fronts in the vicinity of an observation surface. The multifocusing method does not require any knowledge of the subsurface model and can produce an accurate zero offset section, even in cases of a complex geological structure and/or low signal-to-noise ratio. The moveout correction parameters are the emergence angle and the wavefront curvatures for the normal wave and normal-incidence-point wave. The estimated sets of these parameters can be looked upon as new wavefield attributes containing important information regarding the subsurface model. Application of the multifocusing algorithm to synthetic and real data examples demonstrates its advantages in comparison with conventional CMP processing.

Keywords: Seismic data; Multifocusing method; Subsurface imaging

1. Introduction

While depth imaging plays an increasing role in seismic data processing, imaging in time domain still remains an important exploration tool. Experience shows that time imaging provides sufficient information for a variety of subsurface models of moderate complexity. Moreover, even for more complex models that warrant the use of prestack depth migration, time imaging usually constitutes a key first step, which facilitates the estimation of the macrovelocity model for depth imaging.

For these reasons, improving the quality of time sections remains the focus of intensive research. In particular, a lot of efforts are directed towards improving the accuracy of normal moveout (NMO) correction. Indeed, it has long been recognized (Taner and Koehler, 1969) that, even for a horizontally layered and isotropic overburden, the standard Dix NMO equation

$$t = \sqrt{t_0^2 + \frac{x^2}{V_{\mathrm{RMS}}^2}} \tag{1}$$

is a second-order approximation (in offset) of the full travel time expansion which can be represented by an infinite even-powered Taylor series. In Eq. (1), t is the travel time from the source to the reflector and back to the receiver, t_0 is the vertical travel time from the surface to the reflector, x is the distance from the shot to

* Corresponding author. Fax: +972-8-9208811; e-mail: evgeny@gii.co.il

[1] E-mail: boris@gii.co.il.

0926-9851/99/$ - see front matter
PII: S0926-9851(99)00041-5

the receiver (offset), and V_{RMS} is the root-mean-square velocity. The use of higher-order approximations of such a series for NMO correction is also possible, see, e.g., May and Straley (1979). Such approximations proved to be useful for the analysis of individual CMP records, e.g., for AVO analysis, see Gidlow and Fatti (1990) and Ross (1997). However, such approximations found little use in stacking procedures, mainly because with the multi-parameter search based on the same amount of data (CMP gather) the stacking procedure becomes less robust. An alternative approach to NMO correction was proposed by de Bazelaire (1988), using the so-called shifted hyperbola equation

$$t = t_0 - t_p + \sqrt{t_p^2 + \frac{x^2}{V^2}} \qquad (2)$$

which was first proposed by Malovichko (1978). For a given t_0, Eq. (2) is an expansion of the travel time with two independent parameters: t_p and V. The travel time approximation given by Eq. (2), when represented as a series in t^2, is exact through fourth order in offset (Castle, 1994) while still retaining hyperbolic character of the travel time. For sufficiently small offsets the parameter V may be replaced by the constant near surface velocity V_0, resulting in a robust single-parameter correlation/stacking procedure known as p-scan (de Bazelaire, 1988). Castle (1994) has argued that the shifted hyperbola equation is the most general practical NMO equation.

Studies of different travel time equations mentioned above were aimed to improve the quality of CMP stack through better alignment of reflection events within a single CMP gather. By contrast, in the multifocusing approach proposed by Gelchinsky et al. (1997), each zero-offset trace is constructed by stacking traces which need not belong to the same CMP gather, but whose sources and receivers are in a certain vicinity of the central point. Since the traces being stacked no longer belong to the same CMP gather, such a procedure requires a more general moveout correction than the one used in the conventional CMP stacking. For a given source–receiver pair the multifocusing moveout equations (based on the spherical representation of wavefronts) express the moveout correction with respect to a zero-offset trace by three parameters measured at the central point. In other words, the moveout correction expressed by the multifocusing formulas is a three-parameter expansion of the travel time in the vicinity of the central point. Hence, it is closely related to the paraxial ray approximation (see e.g. Tygel et al., 1997). The three parameters are: the emergence angle β and the radii of curvature R_N and R_{NIP} of the two fundamental wave fronts corresponding to the normal wave and normal-incidence-point wave, respectively (Hubral, 1983).

It has been shown that the multifocusing travel time formulas not only provide an adequate representation of the arrival times for arbitrary source-receiver configurations just like the conventional NMO correction does for CMP gathers, but is in fact more accurate for various earth models. In particular, they are very accurate for a spherical reflector under a homogeneous overburden, and for a smoothly curved dome-like reflector (Tygel et al., 1997). For a single CMP gather, the multifocusing moveout correction reduces to de Bazelaire's ''shifted hyperbola'', Eq. (2), which is known to give a superior approximation of the travel times for a horizontally layered medium than the classical Dix NMO equation (Castle, 1994).

The multifocusing moveout correction presents an appealing basis for a stacking procedure, as it can align reflection events in a large gather of seismic traces which spans over many CMP gathers. However, implementation of the multifocusing method presents a technical challenge, due to the need to estimate several moveout parameters (emergence angle and two curvatures) instead of a single parameter (stacking velocity) in standard NMO velocity analysis. The aim of this paper is to demonstrate the practical feasibility of the multifocusing method,

and to compare the multifocusing time sections with the conventional NMO/DMO stacked sections. The details of the theory of the multifocusing method based on the concept of homeomorphic imaging (Gelchinsky, 1989; Keydar et al., 1996; Gelchinsky and Keydar, 1999) have been presented by Gelchinsky et al. (1997; 1999a; b) and will not be repeated here.

The paper is organized as follows. First, we summarize the equations that describe the multifocusing moveout correction and discuss potential benefits of the method. Then, we point out the problems associated with the implementation of the method, and give a brief description of the algorithm. Finally, we demonstrate how the method works on synthetic and real data examples.

2. Multifocusing moveout correction

Let us consider the ray diagram in Fig. 1. The central ray starts at the point X_0 (which is referred to as the central point) with the angle β to the vertical, hits the reflector Σ at normal-incidence-point (NIP) and returns back to X_0. A paraxial ray from the source S intersects the central ray at the point P and arrives back to the surface at the point G. These two rays define a fictitious focusing wave which initially has the wave front Σ_S, focuses at P, is reflected at the reflector Σ and emerges again at X_0 with the wave front Σ_G. We can write the moveout correction in the form (Gelchinsky et al., 1997; Berkovitch et al., 1998):

$$\Delta\tau = \frac{\sqrt{(R^+)^2 + 2R^+\Delta X^+ \sin\beta + (\Delta X^+)^2} - R^+}{V_0} + \frac{\sqrt{(R^-)^2 + 2R^-\Delta X^- \sin\beta + (\Delta X^-)^2} - R^-}{V_0} \tag{3}$$

where

$$R^+ = \frac{1+\sigma}{\frac{1}{R_N} + \frac{\sigma}{R_{NIP}}}, \tag{4}$$

$$R^- = \frac{1-\sigma}{\frac{1}{R_N} - \frac{\sigma}{R_{NIP}}}, \tag{5}$$

and σ is the so-called focusing parameter given by

$$\sigma = \frac{\Delta X^+ - \Delta X^-}{\Delta X^+ + \Delta X^- + 2\dfrac{\Delta X^+ \Delta X^-}{R_{NIP}} \sin\beta}. \tag{6}$$

In the above equations, ΔX^+ and ΔX^- are the source and receiver offsets for a given ray with respect to the central ray, R^+ and R^- are the radii of curvature of the fictitious wave fronts Σ_S and Σ_G in the vertical plane, respectively, and V_0 is the near surface velocity which is assumed constant along the horizontal observation line. Finally, R_N and R_{NIP} denote the radii of curvature of the two fundamental wave fronts corresponding to the normal (N) wave and NIP wave, respectively (Hubral, 1983). The wavefront of the N-wave front is formed by normal rays emitted by different points on the reflector (like in an ''exploding reflector'' scenario), see Fig. 2. The NIP wave front is formed by a point source placed at the point where the zero-offset ray emitted from the central point hits the reflector, see Fig. 3.

The double-square-root Eq. (3) can be understood using the concept of an *auxiliary medium* (Perroud et al., 1999), which can be defined as a

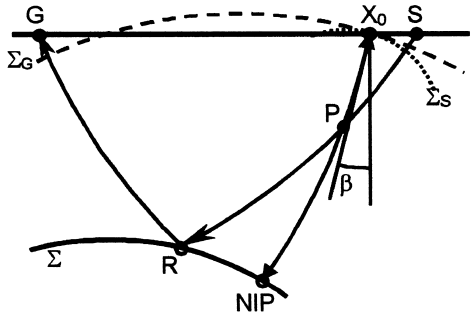

Fig. 1. Ray diagram showing the construction of the focusing wave.

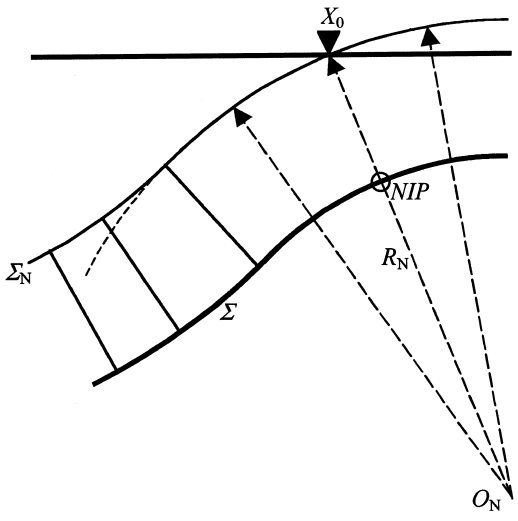

Fig. 2. Wavefront Σ_N of the normal wave produced by a curved reflector Σ under a homogeneous overburden.

homogeneous medium with the velocity equal to the near-surface velocity V_0. In the auxiliary medium, both the central and paraxial rays will be represented by combinations of straight line segments. Consider again the ray diagram in Fig. 1. The first term in the right-hand side of (3) corresponds to the time along the ray segment SP which can be obtained from the triangle SPX_0. The second term corresponds to the time along the ray PRG, and can be obtained from a similar consideration involving the imaginary source P' (image of the focusing point P in the mirror Σ, again, in the auxiliary medium). Point P' is the center of curvature for the fictitious wavefront Σ_G the same way as P is the center of curvature for the wavefront Σ_S.

Quantities R^+ and R^- involved in Eq. (3) are radii of curvature of the fictitious wave fronts Σ_S and Σ_G. It is clear from Fig. 1 that, for a given central ray, the radii R^+ and R^- depend upon the position of the point P where the paraxial ray intersects the central ray and thus upon the position of the source and receiver that define the paraxial ray. Eq. (4) and (5) give the radii of curvature of the fictitious wavefronts R^+ and R^- via the fundamental radii of curvature R_{NIP} and R_N, which are defined by the central ray only and are the same for all the source–receiver pairs in the vicinity of the central ray. The dependence of the radii R^+ and R^- on the position of the source and receiver (or on the position of the point P on the central ray) is contained in the focusing parameter σ which has a very clear physical interpretation. In particular, $\sigma = 0$ means that $R^+ = R^- = R_N$, which implies that point P coincides with the centre of curvature of the normal wave front (or of the reflector), and corresponds to the case of coinciding source and receiver (zero-offset configuration). The cases $\sigma = 1$ and $\sigma = -1$ imply $R^- = 0$ and $R^+ = 0$, and correspond to the common-source and common-receiver configurations. The case $\sigma = \infty$ leads to $R^+ = R^- = R_{NIP}$, and corresponds to the situation where the focusing point P coincides with NIP.

In the general case of a curved reflector and inhomogeneous overburden, Eq. (6) for the focusing parameter σ was derived by Gelchinsky et al. (1997; 1999a; b) as a small-offset approximation. However, for a plane (horizontal or dipping) reflector under a homogeneous overburden, Eq. (6) is exact for all offsets, see Appendix A.

The moveout correction defined by Eqs. (3)–(6) can be applied to arbitrary source and receiver offsets as long as the arcs of the fictitious

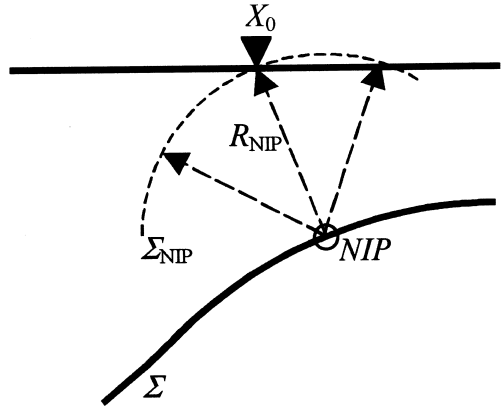

Fig. 3. Wavefront Σ_{NIP} of the NIP wave produced by a curved reflector Σ under a homogeneous overburden.

wave fronts Σ_S and Σ_G can be considered circular in shape. The moveout correction in Eq. (3) is a sum of two hyperbolas. However, for a number of most common source-receiver disbtributions this correction reduces to a single hyperbola. For a common source (common receiver) gather this can be readily seen by substituting $\Delta X^+ = 0$ ($\Delta X^- = 0$) in Eq. (3). For a CMP gather the multifocusing moveout formula (3) reduces to the ''shifted hyperbola'', Eq. (2) under an assumption $R_N = \infty$ (see Appendix B).

3. Advantages of the multifocusing method

As mentioned above, the multifocusing moveout correction as defined by Eqs. (3)–(6) can be applied to any trace if its source and receiver are in a certain vicinity of the central point (central point is defined as a point on the observation line, for which we want to obtain the zero-offset trace). Thus, the multifocusing moveout correction can be used to align reflection events in large super-gathers without loss of the spatial resolution. In multifocusing, a super-gather is a set of traces whose sources and receivers are in such a vicinity of the central point, in which wavefront arcs can be approximated by circular arcs. Fig. 4 shows the geometry of a typical super-gather containing traces from five CMP gathers.

Potential benefits of stacking such large super-gathers as compared to the CMP stack are as follows.

· Stacking a large number of traces spanning over many CMP gathers can increase the stacking power as compared to the conventional CMP stack. In the conventional CMP process-

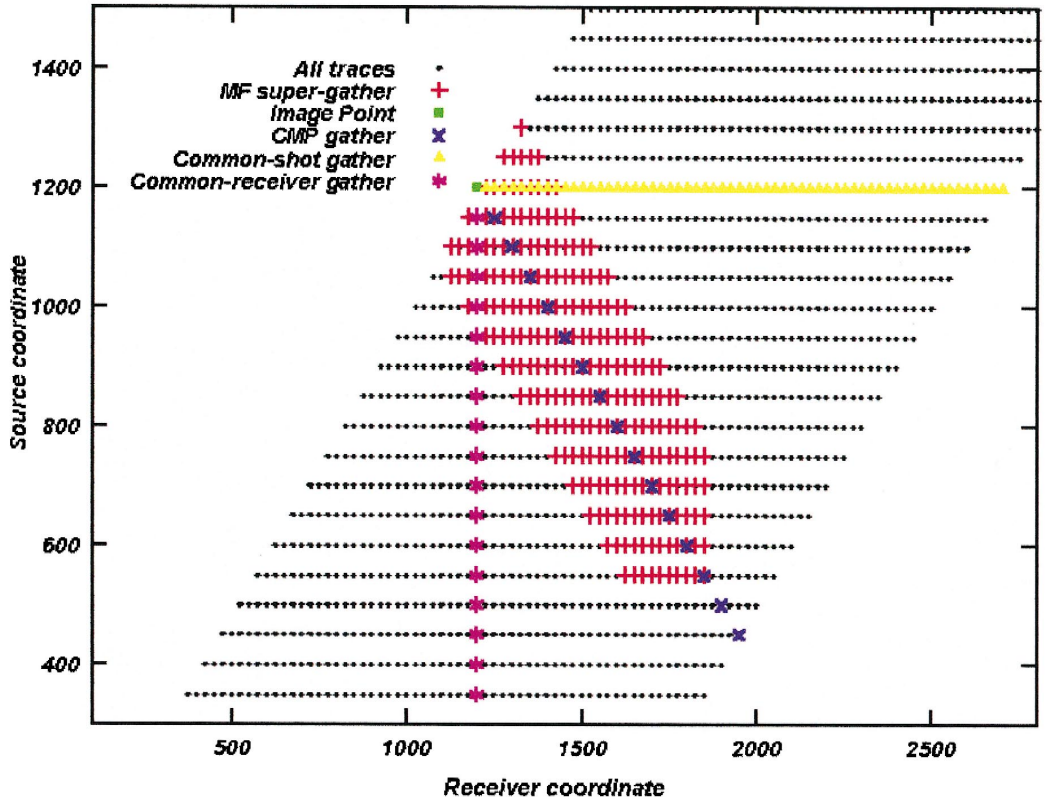

Fig. 4. Multifocusing stacking chart in shot/receiver coordinates. The number of traces in the multifocusing super-gather (red crosses) is many times that in a CMP or common-shot, or common receiver gather.

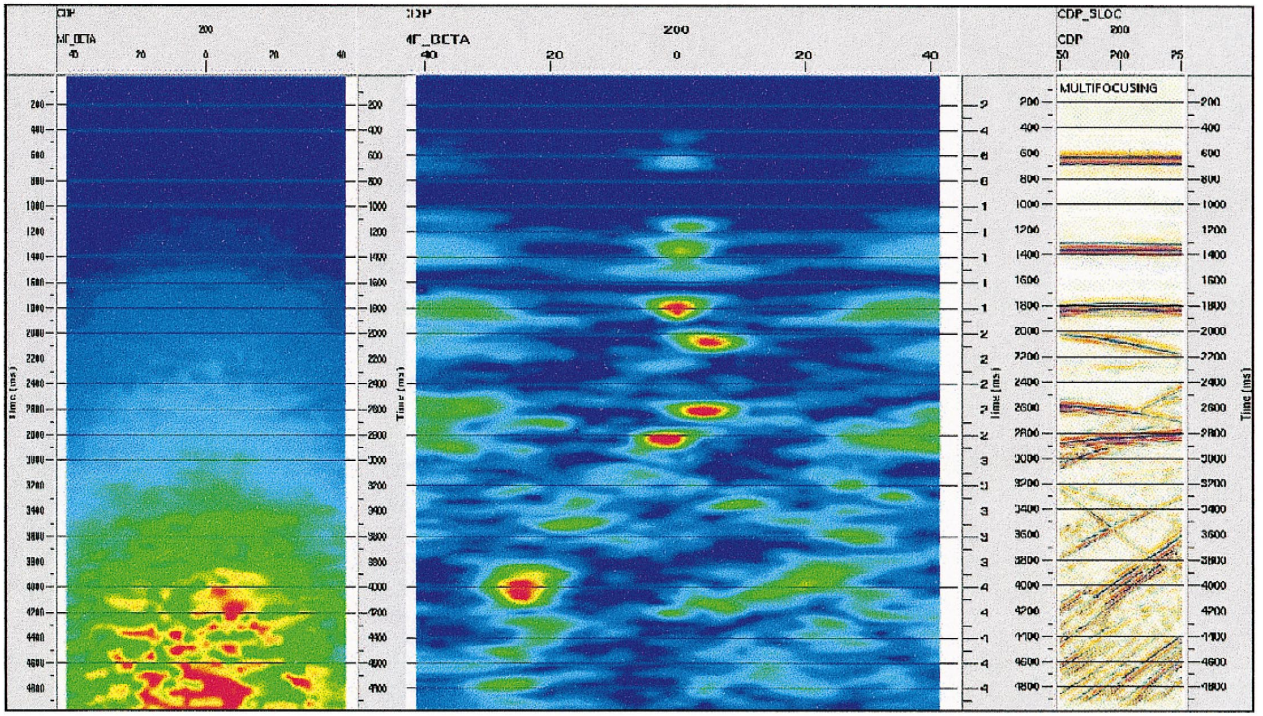

Fig. 5. Multifocusing parameter estimation. Elf's synthetic model. Let panel: NIP wavefront radius vs. t_0 and angle; central panel: semblance vs. t_0 and angle; right panel: the corresponding fragment of the multifocusing stacked section.

ing, the stacking power is defined by the number of traces in a CMP gather, and, ultimately, by the acquisition fold. In multifocusing, the stacking power depends upon the number of traces in the super-gather. This is a user-defined parameter unrelated to the acquisition fold and is limited only by the initial assumptions (circular shape of wavefront arcs within the aperture) and the computational cost. Typically, the number of traces in the super-gather exceeds the acquisition fold at least by an order of magnitude. This can be particularly beneficial for data with low fold and/or low signal-to-noise ratio.

• For a flat reflector under a homogeneous overburden, the NIP radius depends upon the distance between the central point and the reflector and is independent of the reflector dip. For an inhomogeneous overburden R_{NIP} represents the distance between the central point and the reflector in the auxiliary medium, again, irrespective of the dip. Therefore, the events with similar t_0 beneath the same overburden have similar R_{NIP} values irrespective of their dip. Thus, the multifocusing imaging based on the radii of curvature preserves dipping events. Hence, the multifocusing method incorporates the key property of the DMO transform.

• Simultaneous determination of the curvatures and emergence angle makes it possible to recover dip-independent RMS velocities V_{RMS} through a simple algebraic transformation,

$$V_{\mathrm{RMS}}^2 = \frac{2 R_{\mathrm{NIP}} V_0}{t_0}, \tag{7}$$

where t_0 is the zero-offset arrival time at the central point, see Appendix B. These velocities may be used for migration. In this respect the multifocusing method is similar to the DMO velocity analysis (Kessler and Chan, 1993).

• The multifocusing moveout correction (3) for a given sample of the image trace at t_0 depends on the incidence angle and on curvatures measured on seismograms, and does not involve the value of t_0 itself. Thus, all the samples of a given reflection event on a given central trace would have the same parameters within the duration of the wavelet, and hence

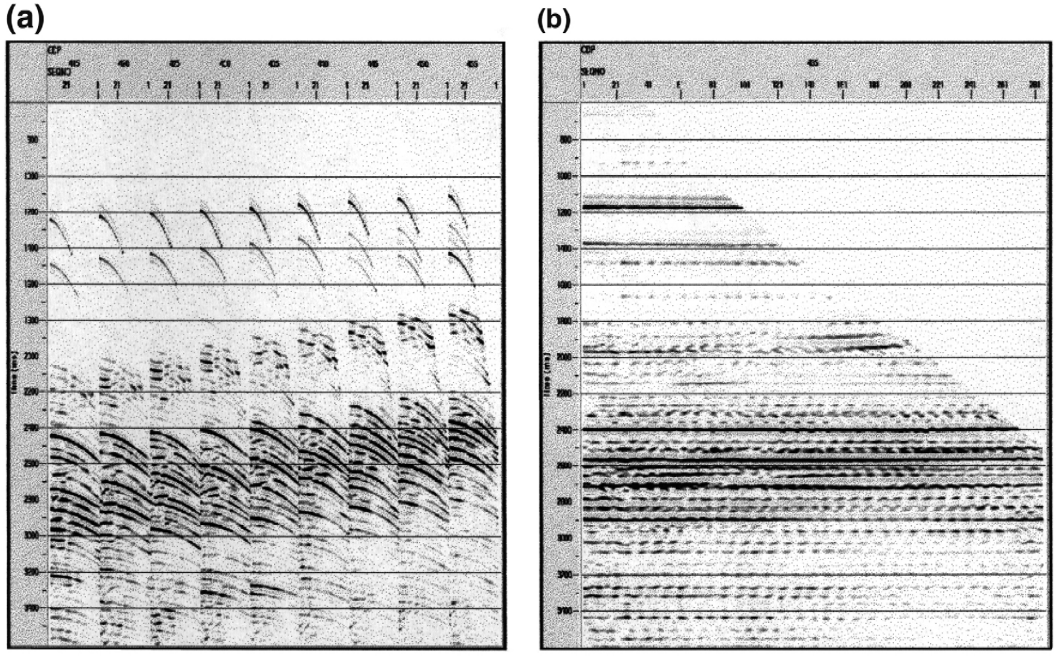

Fig. 6. A super-gather before (a) and after (b) the multifocusing moveout correction. Elf's synthetic model.

the moveout correction will be constant along the wavelet. Thus, the multifocusing moveout correction does not cause the phenomenon known as ‘‘NMO stretch’’.

• The estimation of the multifocusing moveout parameters (analog of velocity analysis in CMP processing) is performed in an automatic manner.

4. Implementation

As discussed above, the multifocusing moveout correction provides an appealing basis for an imaging procedure. However, despite the potential advantages of the multifocusing approach, its practical use in processing of real data has been held back partly by the difficulties of implementation. Indeed, it requires, for each t_0 on each zero-offset trace, determination of three imaging parameters: β, R_{NIP} and R_{N} instead of a single parameter (stacking velocity) in the conventional NMO stack. For the NMO stack the stacking velocity is usually determined by means of an interactive velocity analysis, consisting in displaying a panel of correlation measure (e.g., semblance) as a function of t_0 and velocity, and manual picking of the appropriate correlation maxima as a function of t_0. For the multifocusing parameters a similar procedure is out of the question for two reasons. First, the cost of calculating the correlation measure for all possible combinations of three parameters over a large super-gather is prohibitively high. Secondly, even if such computation were possible, an interactive procedure

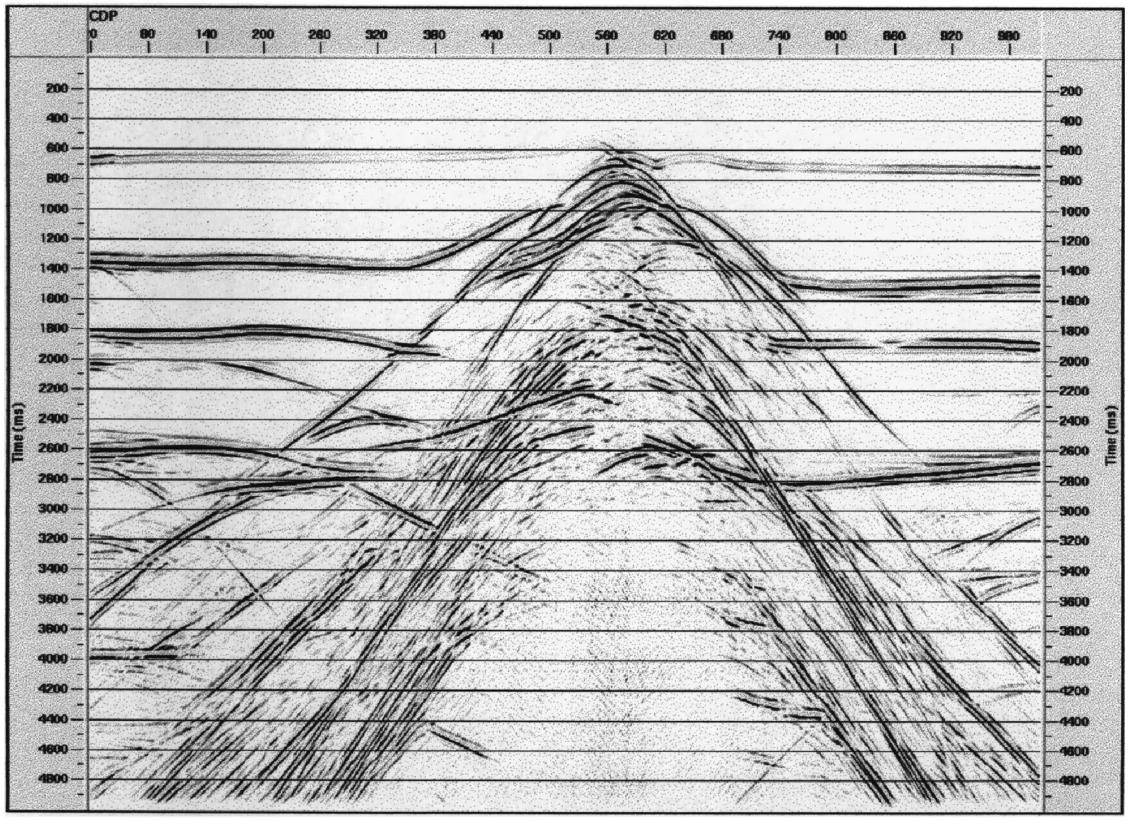

Fig. 7. Multifocusing stacked section. Elf’s synthetic model.

would have to involve displaying and picking maxima of the correlation measure as a function of four variables (t_0 and three imaging parameters), which does not look practical.

Thus, the determination of the imaging parameters must involve some kind of automation, based on optimization methods. This, in turn, brings about all sorts of problems associated with automatic stacking procedures, which have been encountered before in numerous attempts to construct an automatic NMO stack. The main problem is that any automatic stacking procedure optimally collects useful signal as well as spatially correlated noise. The correlation measure as a function of parameters may not be unimodal, thus requiring a global optimization strategy. However, even the global maximum may be related to some kind of coherent noise rather than to the desired signal. For example, strong multiple reflections may have a higher correlation measure than weaker primary events. In the interactive coherence analysis this ambiguity is resolved manually by picking the right maxima on the basis of a priori velocity information. In the optimization process the only possibility is to impose a priori constraints on the imaging parameters. Such a constrained optimization procedure has been employed in our implementation.

Implementation of the multifocusing method is based on the coherence analysis of the signal on the observed seismic traces. The data are moveout corrected along different travel time curves to find the curve closest to the travel time curve of the signal. The unknown parameters β, R_{NIP}, and R_{N} are estimated by finding a

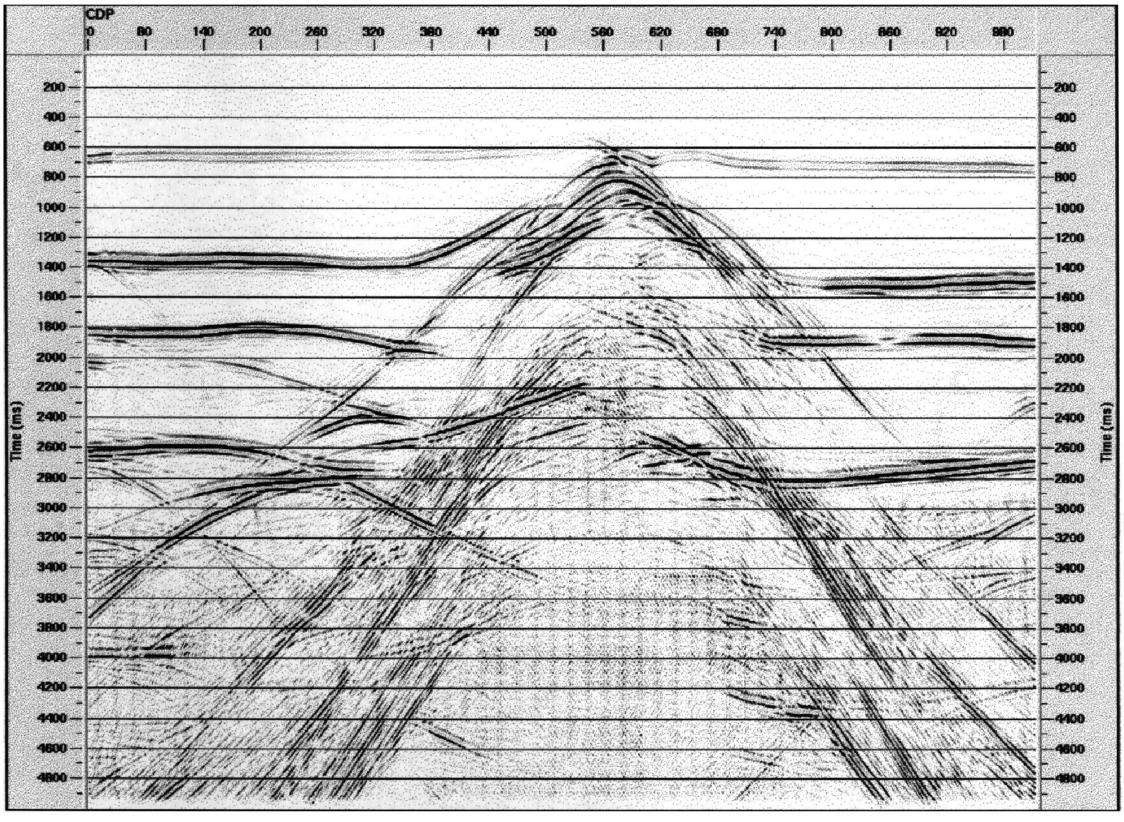

Fig. 8. CMP stacked section after NMO and DMO corrections. Elf's synthetic model.

set of parameters which maximizes the semblance function. Semblance is calculated over the super-gather in a specified time window along the trial travel time curve. Maximization of the semblance is achieved by a nonlinear global optimization method.

The correlation procedure described above is repeated for each central point and for each time sample forming a multifocusing time section. Each sample on this section represents the optimal stacked value corresponding to the optimal values of β, R_{NIP} and R_N. Estimated sets of parameters can also be displayed in space and time forming so-called anglegram $\beta(x,t_0)$ and radius-grams $R_{NIP}(x,t_0)$, and $R_N(x,t_0)$. These three additional sections provide new physically sound wavefield attributes which may aid the interpretation and inversion.

5. Synthetic example

Firstly, the application of multifocusing will be demonstrated on a synthetic data set provided by Elf Aquitaine Production. The panels in Fig. 5 illustrate the parameter estimation in

a)

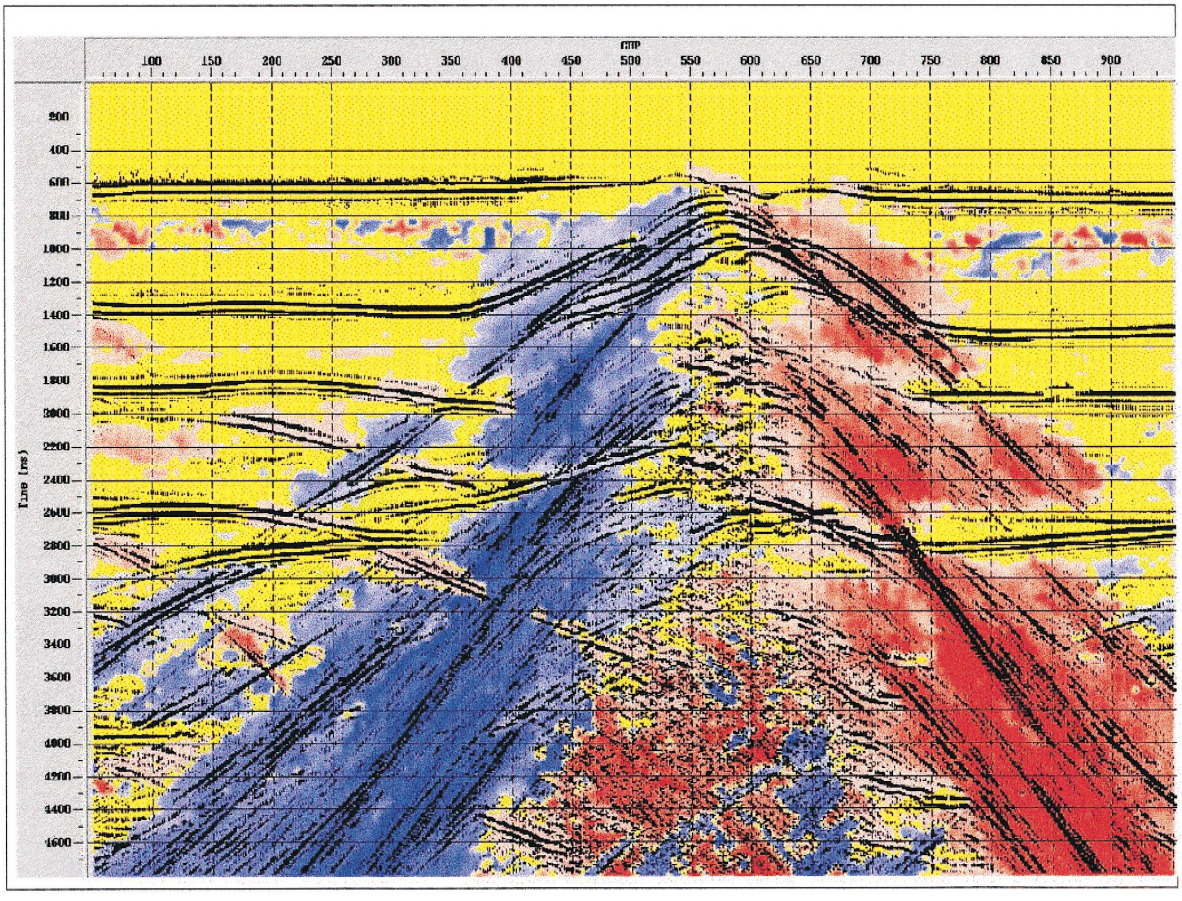

Fig. 9. Time–space distribution of multifocusing moveout parameters for Elf's synthetic model. (a) Emergence angle. Blue: negative, red: positive values; (b) NIP wavefront radius. Blue: low values, red: high values; (c) Normal wave front radius. Blue: positive curvature, red: negative curvature, yellow: flat.

the multifocusing method. In this figure, the central panel shows the semblance as a function of t_0 and emergence angle. Areas of high semblance clearly correspond to the dips visible on the fragment of the stacked section (right panel). The left panel shows the NIP wave front radius as a function of t_0 and angle.

The panels in Fig. 5 illustrate the automatic procedure used by the multifocusing algorithm to find the set of parameters β, R_{NIP}, and R_N that maximizes the coherence criterion. These parameters are then utilized in the multifocusing moveout correction, which is applied to each super-gather. Fig. 6 shows a typical super-gather before and after multifocusing moveout correction.

In this example, the original super-gather (left) comprises traces from nine CMP gathers (60 traces each). The right panel in Fig. 6 shows the same super-gather after multifocusing moveout correction. We see that all reflection events are nearly perfectly aligned across all 540 traces. Stacking these traces increases the stack power by a factor of nine — and that could be made much larger, depending on the number of traces in super-gathers.

Fig. 7 shows the multifocusing section obtained through this procedure. For comparison, Fig. 8 shows a conventional NMO + DMO stacked section obtained after a detailed velocity analysis. One can see a noticeable improvement of multifocusing section compared with the con-

b)

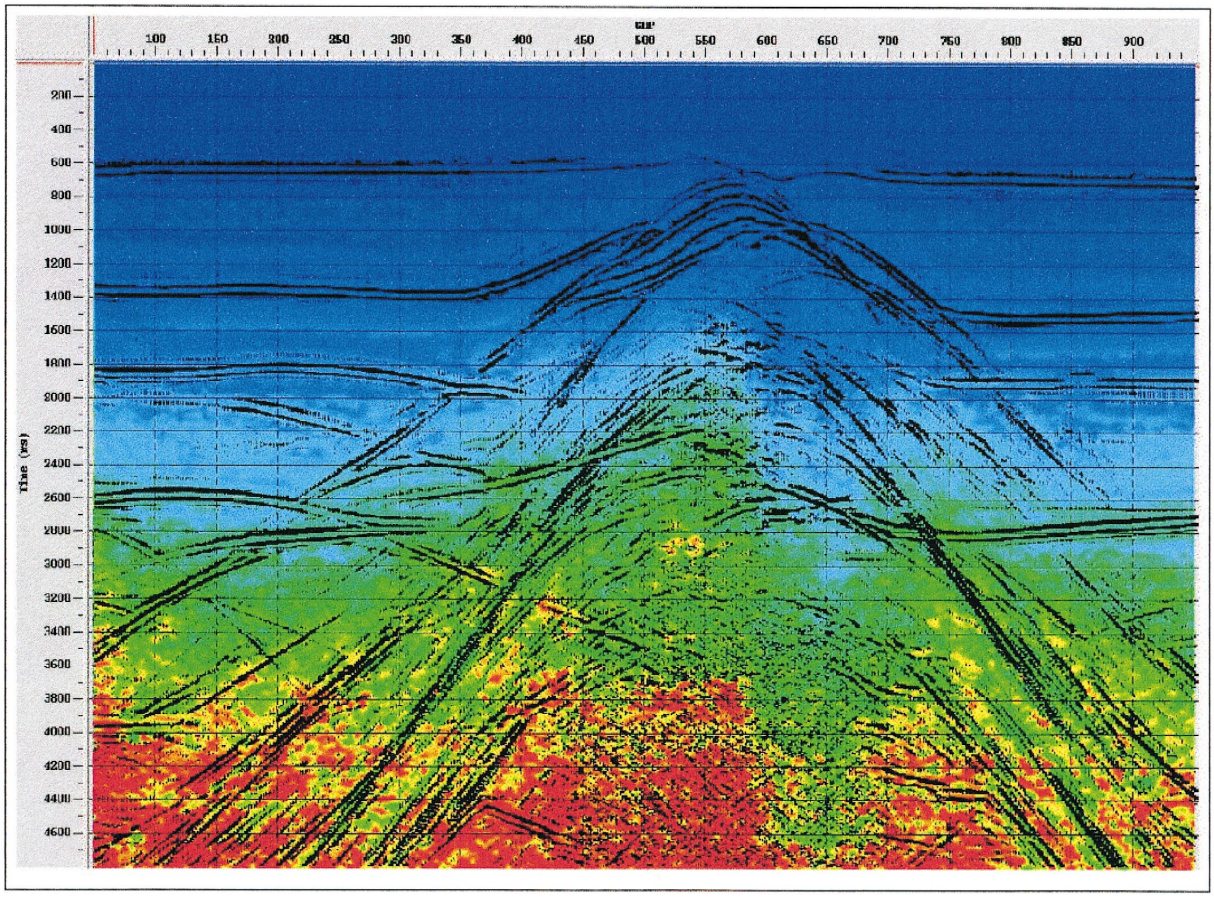

Fig. 9. (continued).

ventional section. Furthermore, the multifocusing moveout parameters — curvatures and emergence angles — are themselves important quantities. Fig. 9 shows the distribution of these parameters on the background of the multifocusing section. Fig. 9a shows the emergence angles. In this figure, red and blue colours correspond to positive and negative dips, respectively, while yellow colour indicates horizontal events. Fig. 9b shows the radius of wavefront curvature for the Normal Incidence Point wave (R_{NIP}). As expected, R_{NIP} rapidly increases with depth. Finally, Fig. 9c shows the wavefront curvature for the Normal wave (R_N). One can see that its behavior is quite different: the largest values correspond to flat events while the lowest indicate regions of curved interfaces or bending points.

The multifocusing parameters provide valuable information which can aid interpretation of time sections and/or assist further processing. In particular, multifocusing parameters can be used to estimate the dip-independent RMS velocity for time migration.

6. Real data example

The next example is a land dataset from Canadian foothills donated by Husky Oil for use

c)

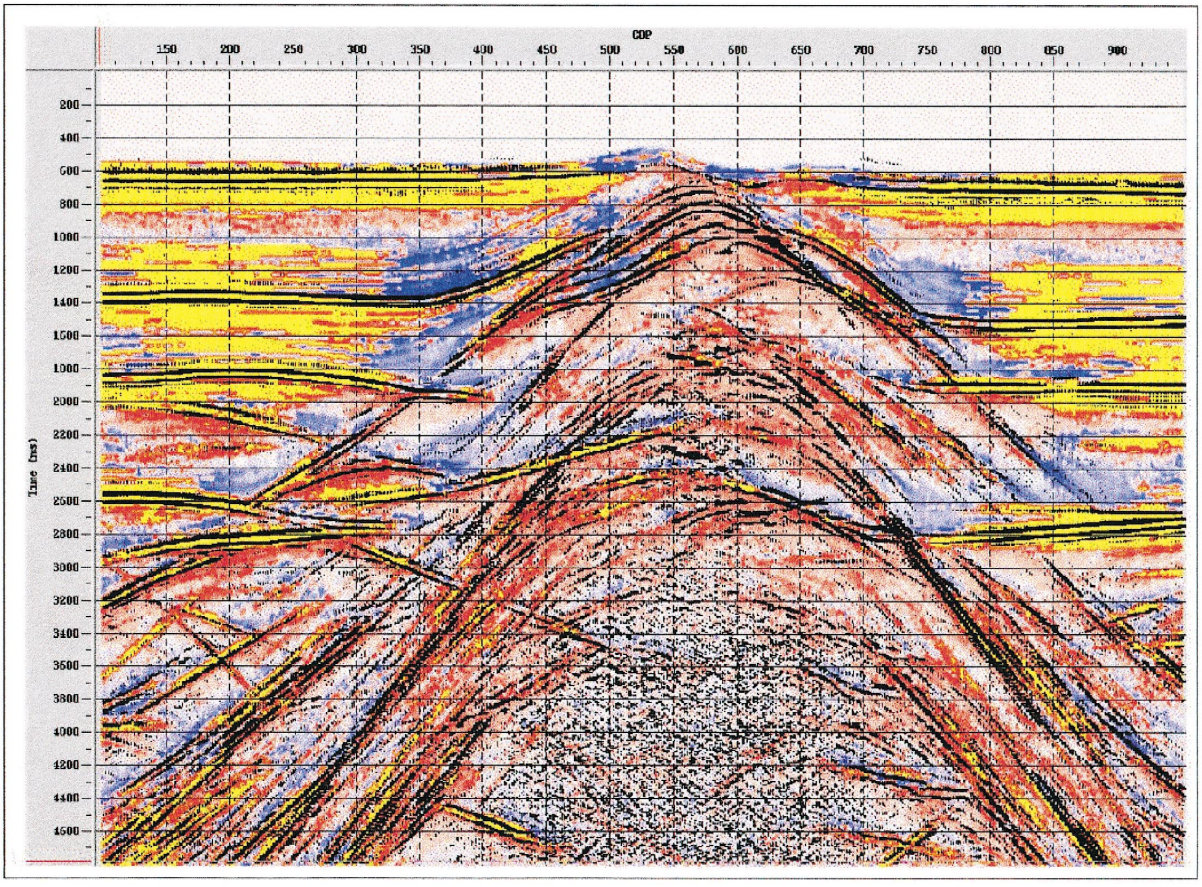

Fig. 9. (continued).

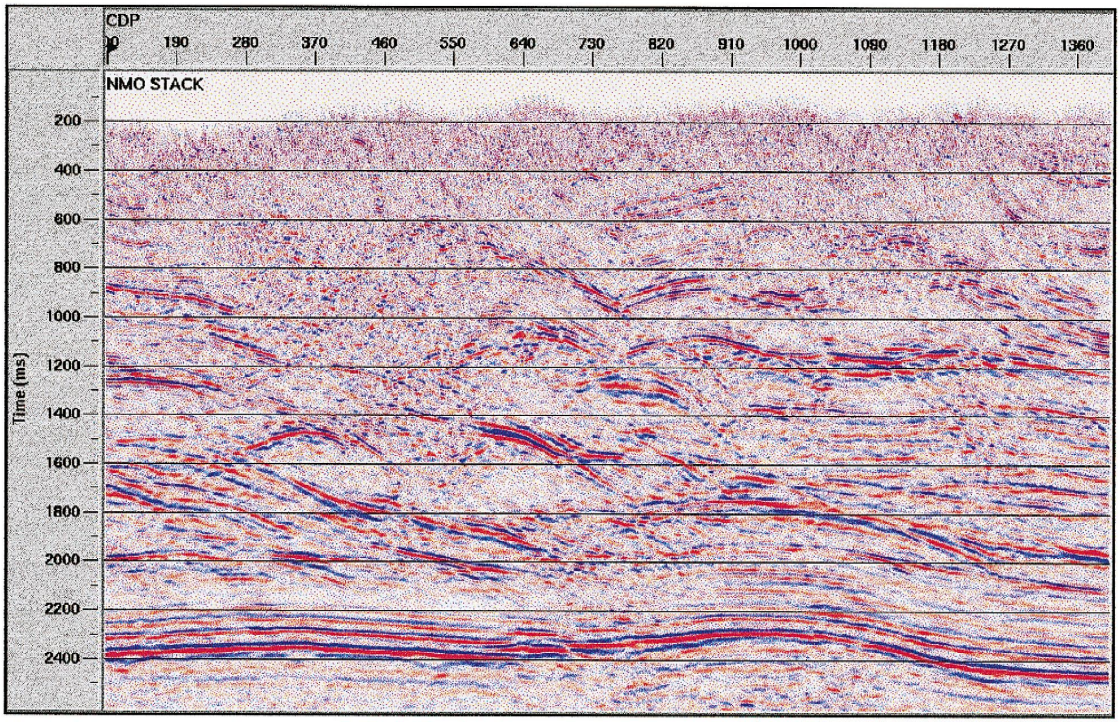

Fig. 10. Conventional NMO + DMO stacked section. Husky Oil example.

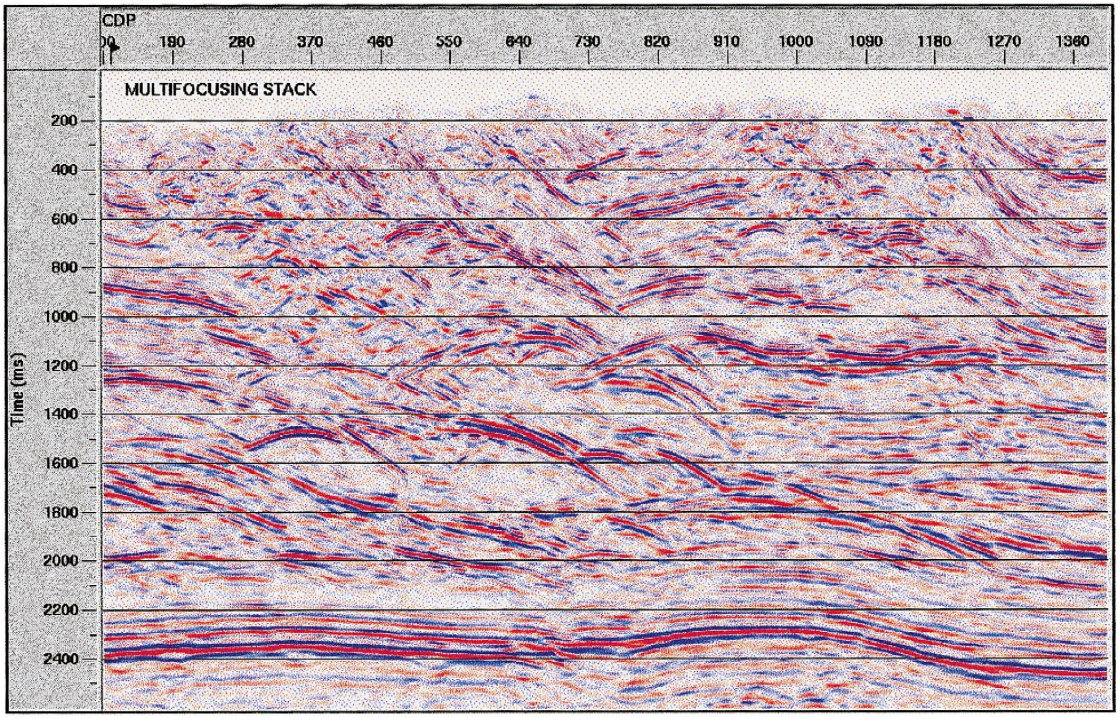

Fig. 11. Multifocusing time section. Husky Oil example.

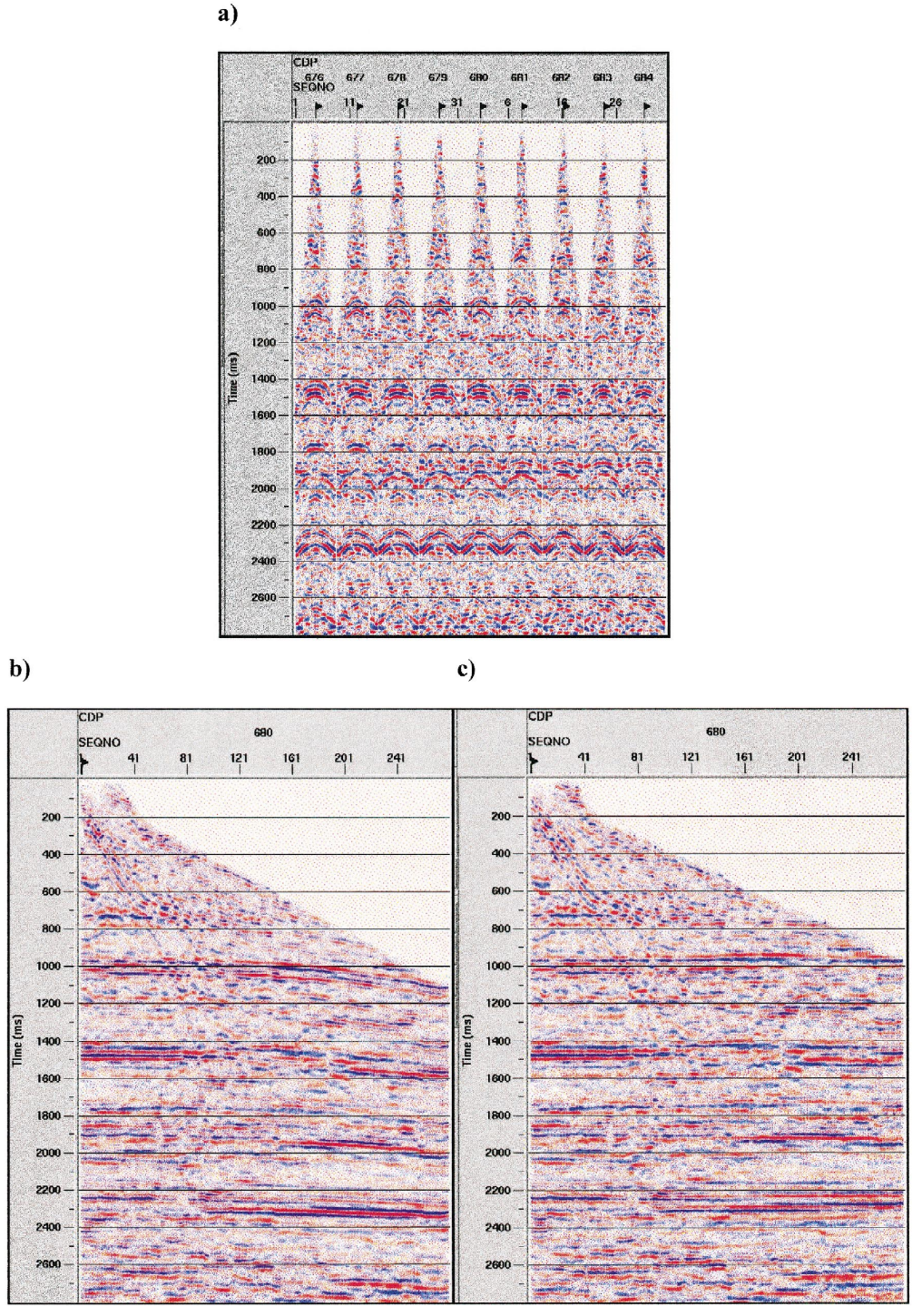

Fig. 12. Input CMP gathers (a), super-gather before (b) and after (c) the multifocusing moveout correction. Husky Oil example.

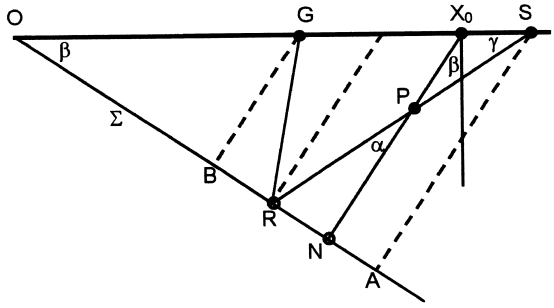

Fig. 13. Ray diagram for a flat dipping reflector under a homogeneous overburden.

in an SEG convention workshop. Fig. 10 shows the CMP stacked section obtained after a detailed velocity analysis with DMO. Fig. 11 shows the multifocusing stacked section. One can see a substantial improvement over the conventional section. This improvement can be explained as follows.

The conventional stacked section has rather low signal-to-noise ratio, especially in the upper part. This was probably caused by a rather small fold in the data. Fig. 12a shows nine CMP gathers of 30 traces each. For the conventional CMP stack, each of these gathers is individually stacked after NMO and DMO.

In the multifocusing approach, these gathers are combined into a single super-gather. Such a super-gather, consisting now of 280 traces, is shown in Fig. 12b. Fig. 12c shows the same super-gather after the application of the multifocusing moveout correction. One can observe a nearly perfect alignment of many reflection events. Flattening of such a large super-gather which spans over many CMPs was achieved by the automatic multifocusing parameter estimation. This ensures an increase of the stacking power of multifocusing over a conventional stack by a factor of nine!

7. Conclusions

We have implemented a new zero-offset stacking algorithm called multifocusing. The multifocusing method consists in stacking seismic data with arbitrary source–receiver distribution according to a new multifocusing moveout correction. We have demonstrated that the multifocusing method can produce a zero offset section superior to the NMO/DMO stacked section in an automatic manner. The method is particularly useful in situations of low fold and/or low signal-to-noise ratio. The estimated sets of multifocusing moveout parameters, namely the emergence angle and the wave front curvatures for the normal wave and normal-incidence-point wave, represent new physically founded wavefield attributes that may be useful for further processing steps, interpretation and inversion.

Acknowledgements

Special thanks go to Moshe Reshef of Landmark for his contribution to the software development. We also thank Elf Aquitaine Production for providing the synthetic data set, prepared by IFP. The financial support of the European Commission through Joule Programme, Contract No. JOF3-CT97-0029, is gratefully acknowledged.

Appendix A. Focusing parameter for a plane (dipping) reflector

For the case of a dipping reflector the expression for the focusing parameter can be derived from Eq. (4)

$$R^{+}=\frac{1+\sigma}{\frac{1}{R_{\mathrm{N}}}+\frac{\sigma}{R_{\mathrm{NIP}}}}. \tag{A1}$$

For the flat reflector R_{N} is infinity. Taking this into account and solving for σ yields

$$\sigma=\frac{1}{\frac{R^{+}}{R_{\mathrm{NIP}}}-1}. \tag{A2}$$

Thus, in order to express parameter σ in terms of the signed source and receiver offsets ΔX^+ and ΔX^- we need to express R^+ in terms of $\Delta X^+ = SX_0 = x$ and $\Delta X^- = -X_0G = y$. In Fig. 13, X_0NX_0 is the central ray, and SRG is the paraxial ray. We define

$$h = R_{\mathrm{NIP}} = X_0N$$

and note that

$$R^+ = PX_0,$$

$$R^- = PNX_0 = 2h - R^-.$$

Now, PX_0, can be determined from a triangle PX_0S

$$\frac{PX_0}{\sin\gamma} = \frac{SX_0}{\sin\alpha}.$$

Noting that $\gamma = (\pi/2) - \beta - \alpha$, we obtain

$$R^+ = x\frac{\cos(\alpha+\beta)}{\sin\alpha} = x\left(\frac{\cos\beta}{\tan\alpha} - \sin\beta\right). \tag{A3}$$

Thus we need to express α in terms of x and y. It is easy to see that

$$OX_0 = h/\sin\beta,$$

$$OS = OX_0 + x = SA/\sin\beta,$$

and

$$OG = OX_0 + y = BG/\sin\beta.$$

Thus

$$SA = h + x\sin\beta$$

and

$$GB = h + y\sin\beta.$$

Therefore

$$AB = AR + RB = SA\tan\alpha + GB\tan\alpha$$
$$= [2h + (x+y)\sin\beta]\tan\alpha.$$

On the other hand,

$$AB = (x-y)\cos\beta,$$

so that

$$\tan\alpha = \frac{(x-y)\cos\beta}{2h + (x+y)\sin\beta}. \tag{A4}$$

Substitution of Eq. (A4) into Eq. (A3) yields

$$R^+ = \frac{2x}{x-y}(h + y\sin\beta). \tag{A5}$$

Finally, we combine Eq. (A2) and Eq. (A5) to obtain Eq. (6).

Appendix B. Multifocusing formula for a single CMP gather and $R_N = \infty$

The purpose of this appendix is to show that for a single CMP gather and $R_N = \infty$ the multifocusing moveout formula (3) reduces to the ''shifted hyperbola'', Eq. (2). To do this, we first rewrite multifocusing moveout formula (3) in a form

$$\tau = \frac{1}{V_0}[(S^+ + S^-) - (R^+ + R^-)], \tag{B1}$$

where

$$S^{\pm} = \sqrt{(R^{\pm})^2 + 2R^{\pm}\Delta X^{\pm}\sin\beta + (\Delta X^{\pm})^2}. \tag{B2}$$

For a CMP gather we can write

$$\Delta X^+ = -\Delta X^- = L.$$

Taking into account that $R_N = \infty$, we can rewrite Eq. (6) in the form

$$\sigma = -\frac{R_{\mathrm{NIP}}}{L\sin\beta}.$$

Then, Eqs. (4) and (5) simplify to

$$R^{\pm} = R_{\mathrm{NIP}} \mp L\sin\beta.$$

Substituting this expression into Eq. (B2) yields

$$S^{\pm} = \sqrt{(R_{\mathrm{NIP}})^2 + L^2\cos^2\beta}.$$

Thus

$$S^+ + S^- = 2\sqrt{(R_{\mathrm{NIP}})^2 + L^2\cos^2\beta}$$

and

$$R^+ + R^- = 2R_{\mathrm{NIP}}.$$

Finally, with the notation

$$\frac{2R_{\mathrm{NIP}}}{V_0} = t_{\mathrm{p}}$$

and

$$2L = x,$$

we obtain

$$\tau = \sqrt{t_{\mathrm{p}}^2 + \frac{x^2\cos^2\beta}{V_0^2}} - t_{\mathrm{p}}$$

or

$$t = t_0 + \tau = t_0 - t_{\mathrm{p}} + \sqrt{t_{\mathrm{p}}^2 + \frac{x^2\cos^2\beta}{V_0^2}}\,. \quad \text{(B3)}$$

Eq. (B3) is a particular variant of Eq. (2) which describes de Bazelaire's ''shifted hyperbola''.

Two simplest cases are of particular interest (de Bazelaire, 1988; Castle, 1994): (1) Homogeneous overburden. Then $R_{\mathrm{NIP}} = h$ is the normal distance between the central point and the reflector, and $t_p = t_0$. Thus

$$t = \sqrt{t_0^2 + \frac{x^2\cos^2\beta}{V_0^2}}\,,$$

which is, of course, the standard NMO hyperbola. (2) Small offsets. The square root in Eq. (B3) can be expressed in powers of x to give

$$t = t_0 + \tau = t_0 - t_{\mathrm{p}} + t_{\mathrm{p}}\left(1 + \frac{x^2\cos^2\beta}{2t_{\mathrm{p}}^2V_0^2}\right)$$

$$= t_0 + \frac{x^2\cos^2\beta}{2t_{\mathrm{p}}V_0^2}\,. \quad \text{(B4)}$$

Comparing this with the standard NMO hyperbola (1) for small offsets

$$t = \sqrt{t_0^2 + \frac{x^2}{V_{\mathrm{NMO}}^2}} = t_0 + \frac{x^2}{2t_0V_{\mathrm{NMO}}^2},$$

we see that the two curves are the same if

$$t_0V_{\mathrm{NMO}}^2 = \frac{t_{\mathrm{p}}V_0^2}{\cos^2\beta},$$

which defines the correspondence between the NMO velocity, R_{NIP} and t_{p}:

$$V_{\mathrm{NMO}}^2 = \frac{t_{\mathrm{p}}V_0^2}{t_0\cos^2\beta} = \frac{2R_{\mathrm{NIP}}}{t_0}\frac{V_0}{\cos^2\beta}, \quad \text{(B5)}$$

or

$$R_{\mathrm{NIP}} = \frac{t_0V_{\mathrm{NMO}}^2\cos^2\beta}{2V_0}. \quad \text{(B6)}$$

For a horizontally layered medium a RMS velocity V_{RMS} can be defined, which can be related to the NIP radius by

$$V_{\mathrm{RMS}}^2 = \frac{2R_{\mathrm{NIP}}V_0}{t_0},$$

or

$$R_{\mathrm{NIP}} = \frac{t_0V_{\mathrm{RMS}}^2}{2V_0}.$$

References

Berkovitch, A., Keydar, S., Landa, E., Trachtman, P, 1998. Multifocusing in practice. 68th Annual Internat. Mtg., Soc. Expl. Geophys. Expanded Abstracts.

Castle, R., 1994. A theory of normal moveout. Geophysics 59, 983–999.

de Bazelaire, E., 1988. Normal moveout correction revisited: inhomogeneous media and curved interfaces. Geophysics 53, 143–157.

Gelchinsky, B., 1989. Homeomorphic imaging in processing and interpretaton of seismic data — Fundamentals and schemes. 59th Annual Internat. Mtg., Soc. Expl. Geophys. Expanded Abstracts, 983–986.

Gelchinsky, B., Keydar, S., 1999. Homeomorphic imaging approach: theory and practice. J. Appl. Geophys. This issue.

Gelchinsky, B., Berkovitch, A., Keydar, S., 1997. Multifocusing Homeomorphic Imaging: Part 1. Basic concepts and formulae, Transcripts of the special course on Homeomorphic Imaging presented by B. Gelchinsky, Seeheim, Germany.

Gelchinsky, B., Berkovitch, A., Keydar, S., 1999a. Multifocusing Homeomorphic Imaging: Part 1. Basic concepts and formulae. J. Appl. Geophys., this issue.

Gelchinsky, B., Berkovitch, A., Keydar, S., 1999b. Multifocusing Homeomorphic Imaging: Part 2. Multifold data set and multifocusing. J. Appl. Geophys., this issue.

Gidlow, P.M., Fatti, J.L., 1990. Preserving far offset seismic data using nonhyperbolic moveout correction. 60th Annual Internat. Mtg., Soc. Expl. Geophys. Expanded Abstracts, 1726–1729.

Hubral, P., 1983. Computing true amplitude reflections in a laterally inhomogeneous earth. Geophysics 48, 1051–1062.

Kessler, D., Chan, W.-K., 1993. DMO velocity analysis with Jakubovicz's dip-decomposition method. Geophysics 58, 1517–1524.

Keydar, S., Gelchinsky, B., Berkovitch, A., 1996. Common-shot-point stacking and imaging method. Journal of Seismic Exploration 5, 261–274.

Malovichko, A.A., 1978. A new representation of the travel time curve of reflected waves in horizontally layered media. Appl. Geophys. 91, 47–53, in Russian.

May, B.T., Straley, D.K., 1979. Higher-order moveout spectra. Geophysics 44, 1193–1207.

Perroud, H., Hubral, P., Höcht, G., 1999. Common-reflection-point stacking in laterally inhomogeneous media. Geophys. Prospect. 47, 1–24.

Ross, C.P., 1997. AVO and nonhyperbolic moveout: a practical example. First Break 15, 43–48.

Taner, M.T., Koehler, F., 1969. Velocity spectra — digital computer derivation and applications of velocity functions. Geophysics 34, 859–881.

Tygel, M., Müller, Th., Hubral, P., Schleicher, J., 1997. Eigenwave based multi-parameter traveltime expansions. 67th Annual Internat. Mtg., Soc. Expl. Geophys. Expanded Abstracts, 1770–1773.